

HgI₂ Detector with a Virtual Frisch Grid

A. E. Bolotnikov, J. Baker, R. DeVito, J. Sandoval, L. Szurbart

Constellation Technology Corporation
7887 Bryan Dairy Road, 100 Largo, FL33777

Abstract

We investigated the performance of a 3 x 3x 6 mm³ HgI₂ detector with a virtual Frisch grid. A metal shield, separated from the material with a thin layer of dielectric, is deposited on the crystal side surfaces, forming the virtual grid. Detectors with this geometry can be used for fabrication of large-area high-efficiency detector arrays that are currently required for nuclear medicine and radioactive material monitoring. We obtained a moderate energy resolution of ~5% FWHM at 511 keV for the tested detector, which can be explained by the fluctuation of the charge loss due to the electron trapping by the small number but geometrically large defects existing inside the HgI₂ material.

Keywords: HgI₂ detectors; CdZnTe detectors; virtual Frisch grid detectors; energy resolution

1. Introduction

HgI₂ room temperature semiconductors are a promising technique [1] for detecting high-energy gamma rays. However, due to material growth limitations, the yield of good quality HgI₂ crystals with large thickness, >5 mm, and large active area, >1 cm², is currently very low. Most of the commercially available HgI₂ detectors have a thickness less than 2-3 mm. For any particular large area and thick HgI₂ detector, it is almost certain that a notable fraction of the crystal volume will have a very poor response that results in a poor performance of the whole detector. On the other hand, there is a significant demand for large area and thick (~1 cm) position sensitive room-temperature semiconductor detectors for nuclear medicine, in particular for PET systems, surgical probes, and nuclear material monitoring.

One possible solution of this problem is to use the pixel geometry, which gives the capability to exclude the bad areas inside detectors by simply turning off the corresponding pixels. Another approach is to use thick but small area (~3 x 3 mm²) detectors. HgI₂ crystals with such dimensions are available at Constellation Technology Corporation (Constellation). Arrays of such crystals (bars) can be used to build large-area high-efficiency position sensitive HgI₂ detectors. Furthermore, an array of the bar detectors exhibits the same “small pixel effect” that exists in pixel detectors. In fact, by shielding the side surfaces of the individual bars, this effect can be significantly enhanced.

A side surface shielded bar detector is a single carrier device. Its operating principle is based on the fact that most of the electric field lines initiated by uncollected holes are intercepted by the metal layer (electrostatic shield) deposited on the detector side surfaces. In other words, the shielding electrode placed on the detector side surfaces creates a virtual Frisch grid inside the detector that acts like a screening grid inside a conventional ionization chamber. There are many types of devices whose operation is based on this principle: hemispherical detectors [2], two-electrode devices [3], capacitive Frisch grid detectors [4], and even pixel detectors, if adjacent pixels act as a shield. It is important to mention that the side surface leakage current ensures a uniform electric field strength distribution inside the bar detector.

2. Experimental

Three random HgI₂ bar detectors manufactured by Constellation were tested in this work; however, only one of them exhibited a good spectral response. Crystals with the dimensions of 3 x 3x 6 mm³ were cut, polished, and coated with paryline using a standard Constellation technique described elsewhere [5,6]. For these tests, two planar contacts on the top and bottom surfaces of the crystal were simply painted with a conductive paint (see Fig. 1). The side surfaces were first wrapped in a thin layer of a

Teflon[®] tape and above that wrapped with a cooper tape. Each detector was mounted on a small PC board, and three thin wires were glued to its contacts (cathode, anode, and shield). The device was mounted inside a light-protected and electrostatically shielded box containing a standard eV-5093 preamplifier. The data acquisition system included a spectroscopy shaping amplifier, MCA card, digital oscilloscope to store waveforms, and standard NIM electronics. Several radioactive sources: ²²Na, ¹³⁷Cs, and ⁶⁰Co were used to investigate the spectroscopic properties of the bar detector. As is discussed later, it was important to use collimated sources to ensure that photons enter the detector from the cathode side only.

In order to investigate the shapes of the signals produced by incident photons inside the detector at different depths, we used annihilation photons from a ²²Na source and an experimental setup (Fig. 2) which allowed to us to collimate the source, and, at the same time, to trigger interaction events. The setup included a 2" thick NaI scintillating detector located as shown in Fig. 2 and operating in coincidence with the HgI₂ detector. A ²²Na source was placed a few millimeters above the detector (cathode end) and separated by a 2" thick lead collimator (5 mm hole diameter) from the NaI detector. Beta-decay of the ²²Na generates a pair of 511 keV photons escaping the source in opposite directions. If the NaI scintillator detects one photon, then, the second one enters the HgI₂ detector from the cathode side. The event in the scintillator generates a trigger signal with a 0.5 μs wide time window. The time corresponding to the detection of the photon in the HgI₂ crystal is determined with a constant fraction discriminator (CFD). If the CFD output signal arrives within the trigger window, then a coincidence signal is sent to the MCA card or to the digital oscilloscope. By varying the delay time of the trigger one can select events from ~0.5 mm thick slices of the detector located at different distances from the anode.

3. Results and discussions

3.1. Theoretical shape of induced signals

The mathematical problem of finding a potential distribution created by a point-like charge inside a grounded metal box can be solved analytically [7]. The surface density of the charge on the anode plate is directly proportional to the normal component of the electric field strength at the surface. Thus, the total charge induced on the anode can be calculated by integrating over the anode area the normal component of the electric field strength at the anode. Fig. 3 shows the dependence of the total induced charge versus a distance between the anode and the source charge for different ratios of the anode size to the detector height. The same curves represent temporal dependencies of the anode signal (output from a charge-sensitive preamplifier) when the source charge drifts from the cathode toward the anode. As is seen, for small aspect ratios, the majority of the signal is induced near the anode. This illustrates a formation of the virtual grid. Fig. 4 shows the shapes of the signals measured after the charge sensitive preamplifier for different trigger delay times. As is seen, for a 0.5 μs delay time, which corresponds to the interaction points located close to the anode, the signal rises linearly. This means that, if compared with a "classic" gridded ionization chamber, the point of interaction lies between the shielding grid (virtual grid in the case of bar detectors) and the anode. The waveforms acquired for longer delay times are very similar to those shown in Fig. 3, and correspond to the interaction points located between the virtual grid and the cathode. We found experimentally that for 1200 V of cathode bias, the coincidences of NaI and HgI₂ signals take place when the trigger delay times lie between 2.8 and 8.0 μs. This corresponds to an electron drift time of ~5 μs and electron mobility of ~60 cm²/Vs.

3.2. Pulse-height spectra

Figure 4 shows the pulse-height spectrum from a ²²Na source simulated for the bar detector. In the simulation, we used an electron μτ-product of 4×10^3 cm²/V experimentally measured for the tested detector. We also assumed the real geometry of the experimental setup used to measure the energy spectra. As is seen, the energy resolution is determined by the electronic noise only, and is expected to be less than 1% at 662 keV. An experimentally measured spectrum is shown in Fig. 5(a). Fitting the peak gives 6.5% FWHM energy resolution for 511 keV, which is a very good result for a 6 mm thick HgI₂ detector. However, the spectrum looks much worse than the simulated spectrum, although the simulation takes into account the electron trapping effect and real geometry. This means that fluctuations of the charge lost due to random distribution of the points of interactions over the entire detector volume cannot explain the degradation of the spectrum. On the other hand, such degradation could be caused by the interactions

taking place near the side surfaces (where the electric field could be very low) or very close to the anode contact where the shielding efficiency of the virtual grid is poor. By setting the trigger window between 3 and 8 μs we were able to reject all the “slow” and “fast” events. However, despite all this, only a small improvement was observed in the pulse-height spectrum shown in Fig. 5 (b).

To better understand the effects responsible for the degradation of the energy resolution of the tested detectors, we set a 0.5 μs trigger window and selected the events from ~ 0.5 mm thick slices of the detector located at different distances from the anode. Fig. 6 shows a succession of energy spectra corresponding to the events from the different slices (or different trigger delay times). As is seen, the detector response to the interaction events located close to the anode improves except for events that occur very close to the anode, below the virtual grid. The pulse-height spectrum of the events from the layer adjacent to the cathode exhibits the worst resolution. This is illustrated in Fig. 7, which shows the widths (FWHM) and positions of the peaks evaluated from the pulse-height spectra measured for different trigger delay times (or detector layers). The dependence of the peak position versus the delay time allows us to estimate the electron lifetime by fitting the measured curve with an exponential function. We found the electron lifetime to be 58 μs , which is in agreement with the lifetime estimated using a pulse-shape analysis technique for good quality HgI_2 detectors. With such a long lifetime, the spectrum degradation due to trapping should be significantly less than what was observed. Moreover, no changes in the widths of the peaks should be seen for the spectra collected for different delay times (or for the different detector slices). This assumption is a basic principle that is employed in different depth correction techniques developed for CdZnTe and gas filled ionization detectors. In the case of the HgI_2 detector tested here, this assumption seems to be incorrect. It is clearly seen from the spectra in Fig. 6 that the further from the anode the interaction takes place, and the longer the distance traveled by the electron cloud, the stronger the fluctuations in the lost charge due to trapping. In other words, the width of the peaks cannot be explained by fluctuation of the interaction points inside the detector volume that result in the fluctuation of the collected charge. Apparently, fluctuations in electron trapping process are responsible for the large fluctuation of the charge lost due to the electron trapping.

3.3. Factors limiting the energy resolution of HgI_2 detectors

Assume that the total number of the electrons lost due to trapping is N , and each trapping center can only trap a single electron, then the dispersion of the number of the loss charge $D(N)$, simply equals N :

$$D(N)=N. \quad (1)$$

From here one can find the relative fluctuation of the lost charge equal to $(1/N)^{1/2}$. A 511 keV photon creates $N_0 \sim 10^5$ electron-hole pairs in HgI_2 . Since the electron lifetime is 58 μs , the total number of trapped electrons is expected to be $N \sim 10^4$. If it is also taken into account that only 10% of the total charge is lost, then the contribution of the lost charge fluctuations to the detector energy resolution will be less than 0.1%. In contrast, the experimentally measured width of the peaks (see Fig. 7) varies between 3 and 7 % depending on distance from the anode.

The other possibility is to assume that the charge is trapped by a fewer number of centers, but each center traps a large fraction of the charge, e.g., the entire electron cloud could interact with macroscopic crystal defects with a high concentration of accumulated traps. In this case, one can write the total number of the lost electrons as:

$$N = \mathbf{e}n, \quad (2)$$

where \mathbf{e} is the average number of electrons trapped by a single center, n is average number of centers participating in the trapping process during the drifting time. If $1 - \exp(-t/\mu) \sim t/\mu$, then, as a first order of approximation, \mathbf{e} and n can be treated as independent variables. Using the error propagation formula, one can find:

$$D(N)/N^2 = D(\mathbf{e})/\mathbf{e}^2 + D(n)/n^2. \quad (3)$$

where $D(\mathbf{e})$ and $D(n)$ are dispersions of \mathbf{e} and n , respectively.

The width of the peaks, as seen in Fig. 7, increases linearly with delay time. This means the fluctuations of the trapped charge is directly proportional to the distance traveled by the electron cloud, which is equivalent to say that the fluctuations of the trapped charge is directly proportional the total number of trapping centers interacting with the electron cloud, and thus, the second term in (2) can be neglected. If we define σ_E and σ_e as the square roots of $D(E)$ and $D(e)$, respectively, then $\sigma_N = \sigma_e n$. If we assume that $\sigma_e = e^{1/2}$, then one can write the peak widths as:

$$FWHM = 2.36 n e^{1/2}. \quad (4)$$

Substituting $ne = N_{ot}/t$ in (4):

$$FWHM = 2.36 N_{ot}/t e^{1/2}. \quad (5)$$

Using this dependence, we fitted the energy resolution curve shown in Fig. 7. From the fit we found that e is ~ 25 electrons per trapping defect and n is ~ 500 trapping centers per a 6 mm drifting length inside the detector.

This result shows that the electron loss in HgI_2 is not randomly distributed over the crystal volume microscopic trapping centers, e.g., impurity levels, each capable of trapping only a single electron, but rather with macroscopic defects with very high local concentration of trapping centers. This mechanism could also explain the poor energy resolution observed with long-drift $CdZnTe$ detectors described in References [8,9]. In such a case, the depth correction techniques that are normally applied to compensate for charge losses will not help to improve the total energy resolution of the detector.

4. Conclusions

We demonstrated a good response of the $3 \times 3 \times 6 \text{ mm}^3$ HgI_2 detector with a virtual Frisch grid to high-energy gamma rays. The energy resolution was found to be less than 5% FWHM for 511 keV photons, which is a very good result for such a thick HgI_2 crystal, but is still far away from that originally expected for HgI_2 detectors. The deterioration of the energy resolution can be explained by the presence of macroscopic crystal defects, which accumulate a high concentration of electron traps. The fluctuations in the charge trapped by such centers can account for the experimentally measured energy resolution. We estimated that on average the electron cloud created by the incident photon inside the detector interacts with ~ 500 defect centers over a 6 mm drifting length, and that each center traps ~ 25 electrons. It is very tempting to associate these defects with the mosaic nature of HgI_2 material.

Acknowledgments

The authors wish to thank A. Bolozdynya for friendly discussions and comments.

Figures

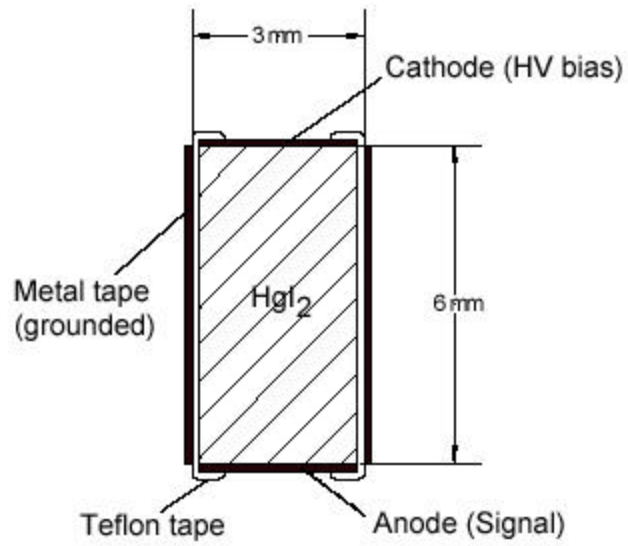


Fig. 1. A schematic of the bar detector with a virtual Frisch grid. For these tests, the detector side surfaces were wrapped with a thin layer of a Teflon tape followed by a cooper tape.

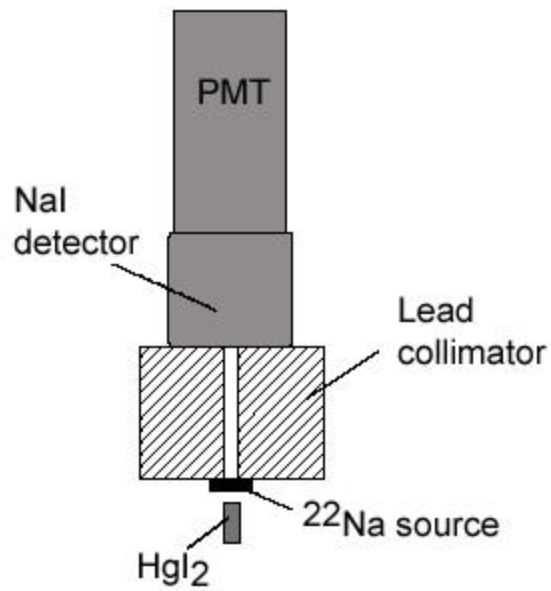


Fig. 2. A schematic of the experimental setup.

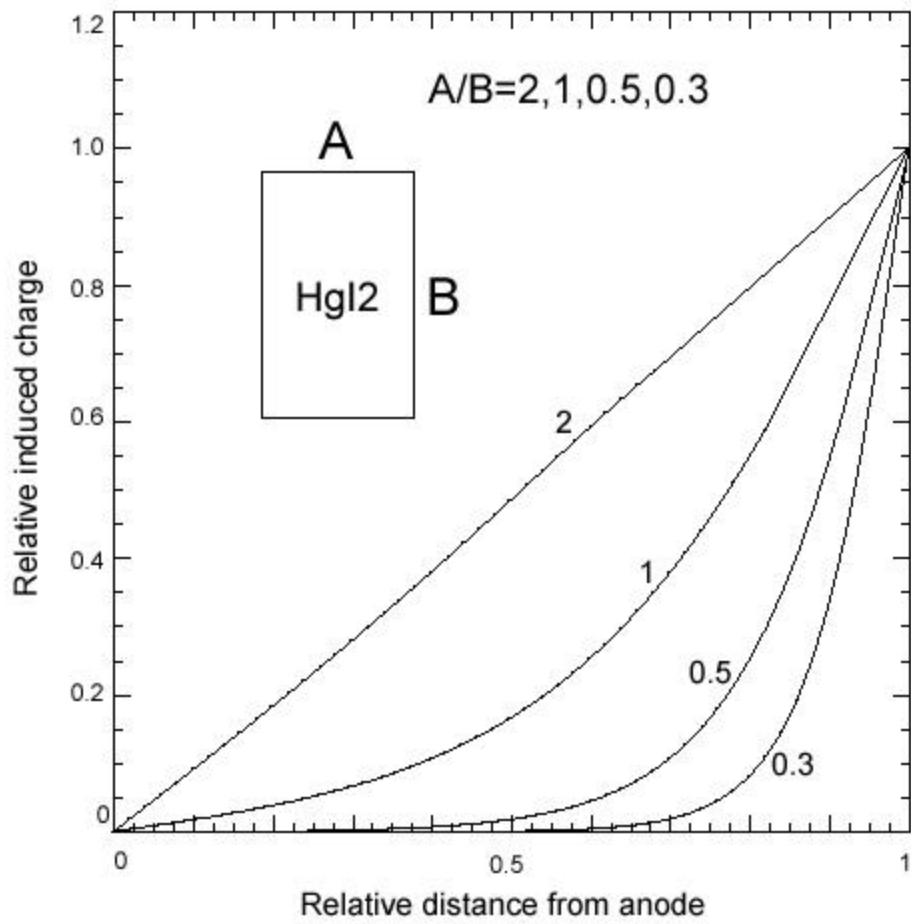


Fig. 3. Dependence of the total induced charge versus distance to the anode for different ratios of the anode size to the detector height.

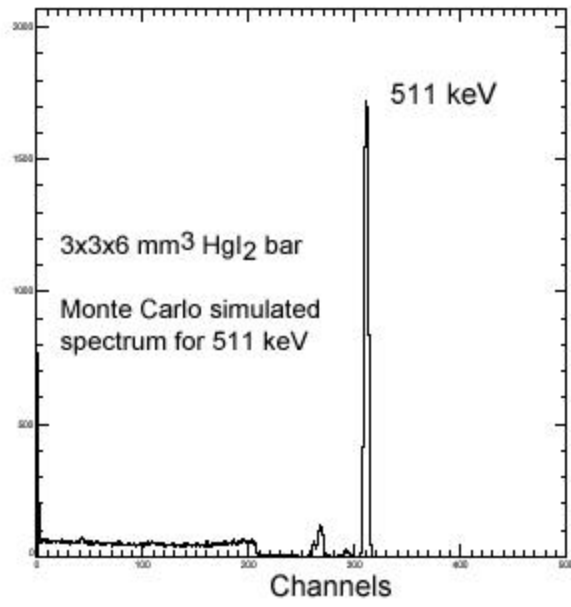


Fig. 4. Monte Carlo simulated pulse-height spectrum from a ²²Na source. A $\mu\tau$ -product is $4 \times 10^{-3} \text{ cm}^2/\text{V}$.

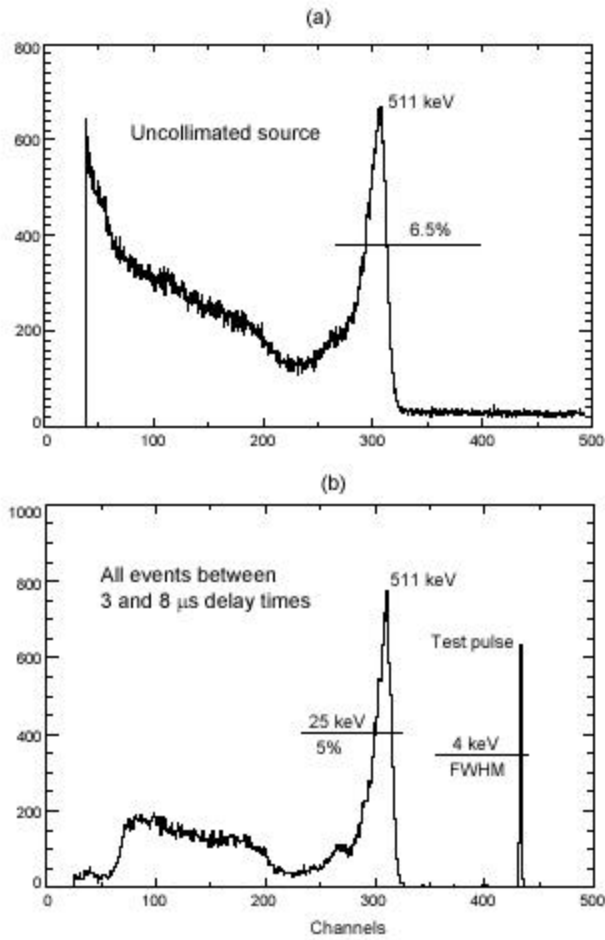


Fig. 5. Experimentally measured pulse-height spectra for the ^{22}Na source located above the cathode side of the detector: all events included (a); events from the 1-mm thick layer adjacent to the anode are rejected (b).

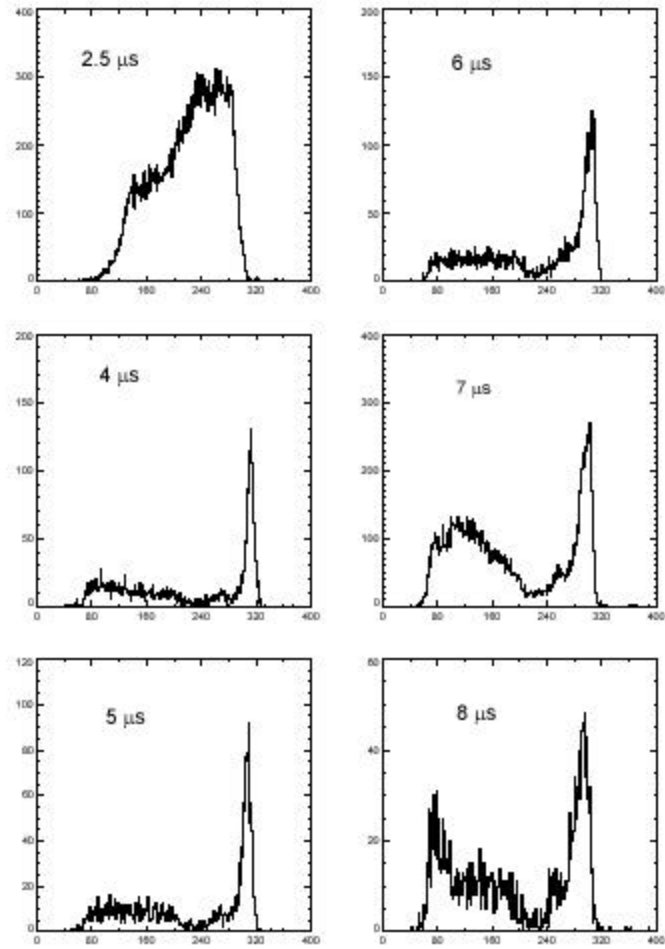


Fig. 6. Succession of pulse-height spectra collected for the events from different 1-mm thick layers inside the detector (or different trigger delay times).

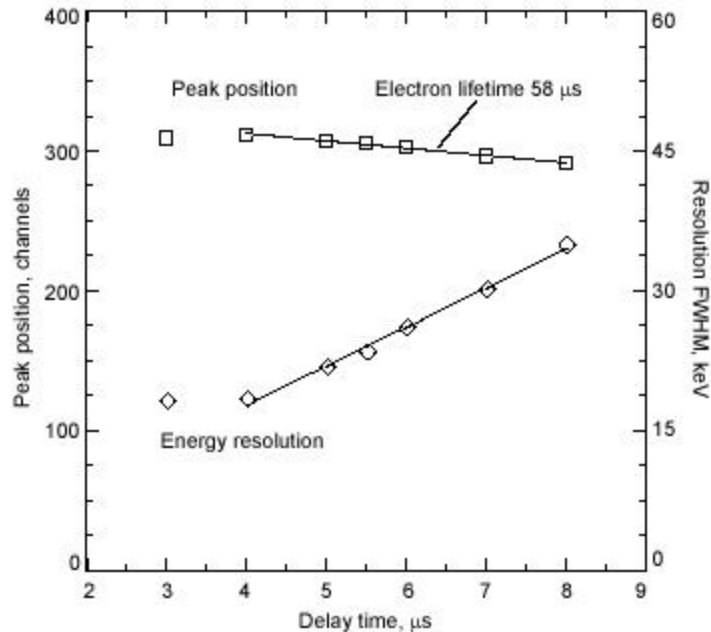


Fig. 7. The width (FWHM) and peak positions evaluated from the pulse-height spectra measured for different layers of the detector (or trigger delay times).

References

- [1] T. E. Schlesinger and R. B. James, Semiconductors and semimetals," in *Semiconductors for Room Temperature Nuclear Detector Applications*, San Diego, CA: Academic, 1995.
- [2] V. Ivanov, A. Loutchanski, "Geometrically weighted CdZnTe Frisch grid nuclear radiation detectors," to be published in *Nucl. Instr. And Meth. A*.
- [3] K. Parnham, C. Szeles, K. Lynn, and R. Tjossem, "Performance improvement of CdZnTe detectors using modified two-terminal electrode geometry," in *Proc. SPIE Conf. Hard X-ray, Gamma Ray and Neutron Detector Physics*, vol. 3768, pp. 49-54, 1999.
- [4] G. Montemont, M. Arques, L. Verger, and J. Rustique, "A capacitive Frisch grid structure for CdZnTe detectors," *IEEE Transactions on Nuclear Science*, vol. 48, n. 3, pp.278-281, 2001.
- [5] A. Gerrish, R. Brogle, R. Johnson, S. Pauly, "Development of a compact mercuric iodide radiation intensity counter," *Nucl. Instr. And Meth., A* 422, pp. 227-231, 1999.
- [6] Lodewijk van den Berg, Ron D. Vigil, "Fabrication of mercuric iodide radiation detectors", *Nucl. Inst. And Meth., A* 458, pp. 148-151, 2001.
- [7] N. N. Lebedev, I. P. Skalskay, J. S. Ufland, "Collection of mathematical physics problems," Moscow, 1955.
- [8] V. Gostilo, C. Budtz-Jorgensen, I. Kuvvetli, D. Gryaznov, I. Lisjutin, and A. Loupinov, "The development of drift-strip detectors based on CdZnTe," *IEEE Transactions on Nuclear Science*, vol. 49, n. 5, pp.2530-2534, 2002.
- [9] A. Shor, I. Mardor, and Y. Eisen, "Performance of 1x1x1 cm³ pixel CdZnTe gamma detectors," *IEEE Transactions on Nuclear Science*, vol. 49, n. 5, pp.1935-1940, 2002.